




Two effects in nucleon-induced nonelastic cross sections based on the intranuclear cascade modelMasahiro Nakano ^{1,2,*}, Yuji Yamaguchi ² and Yusuke Uozumi ²¹*New Medical Statistics Research Institute, 1245-11 Tateiwa, Iizuka, Fukuoka 820-0003, Japan*²*Department of Applied Quantum Physics and Nuclear Engineering, Kyushu University, 744 Motoooka, Nishi-ku, Fukuoka 819-0395, Japan*

(Received 3 April 2020; accepted 15 June 2020; published 10 August 2020)

Proton- and neutron-induced nonelastic cross sections for ^{12}C , ^{27}Al , ^{56}Fe , and ^{208}Pb are investigated in the low-energy region from 100 MeV down to nearly 0 MeV based on a framework of the extended intranuclear cascade (INC) model. It is shown that the present INC model can reproduce the experimental data both for the proton- and for the neutron-induced nonelastic cross sections of a wide range of targets in a systematic way and that the crucial point is to include the suppressed transition probability of the excited particles due to the discrete level constraint. On the basis of the reliability of the INC calculation, we analyze two effects of the discrete level constraint and Coulomb repulsion separately for the proton and for the neutron injection cases, and we elucidate the domain of the target mass and the incident energy where two effects play important roles.

DOI: [10.1103/PhysRevC.102.024608](https://doi.org/10.1103/PhysRevC.102.024608)**I. INTRODUCTION**

The nucleon-induced nonelastic cross section is defined as the total cross section minus the elastic-scattering cross section. It includes all the reactions, such as particle emissions, inelastic scatterings, and absorptions except the elastic scattering. For the description of the nucleon-induced reactions, there are several dynamic models, such as intranuclear cascade model [1], quantum molecular dynamics [2], and antisymmetrized molecular dynamics [3]. Among them, the intranuclear cascade (INC) model is a promising approach to the complex nuclear reactions. Since the original work by Serber [1], a lot of important works have developed the INC model to various applications. Among extensive works, remarkable results have been brought for reactions induced with high-energy nucleons by an early version of the INC of Cugnon [4], and further for reactions induced with light nuclei by the modified version INCL4 coupled to the ABLA evaporation-fission code [5], for photonuclear reactions [6], for spallation reactions [7], and for a lot of applications not mentioned here. Furthermore, the INC model has been extended to the higher-energy range by including multipion production [8]. In addition, Uozumi *et al.* have shown that their INC model followed by the generalized evaporation model [9] has explained the double-differential cross sections for, such as (p, px) , (p, dx) , and $(p, \alpha x)$ in very wide energies and angles [10–13].

Despite the wide applicability of the INC model, there have been opinions on the low-energy limit of the application [14,15]. Confining the discussions to the nucleon-induced nonelastic cross sections, there have been no studies that lead to a reliable prediction of the experimental data in this low-

energy region below a few tens of MeV. Recently, we have shown that the INC can be extended to the low-energy region for the neutron-induced case [16] and for the proton-induced case [17] separately.

Therefore, the main purpose of the present paper is to show the INC model can reproduce the experimental data both for the neutron- and for proton-induced nonelastic cross sections at the same time and for a wide mass range from a light target ^{12}C to a heavy target ^{208}Pb in the low-energy region. The key is to include the effect of the discrete level constraint (DLC) as was pointed out in Refs. [16,17]. The importance of the effect of DLC has been pointed out for the first time in our previous paper [16] for an explanation of the neutron-induced nonelastic cross sections in the very low-energy region below 20 MeV. As for proton-induced nonelastic cross sections, it is difficult to verify the existence of DLC since there is the effect of Coulomb repulsion which brings a similar incident energy dependence in the cross sections. In the previous paper [17], we have proven that only Coulomb repulsion is not sufficient to reproduce the experimental tendency by using a scaling law of the charge and the incident energy, and the INC model including two effects of the discrete level constraint and the Coulomb repulsion can reproduce the experimental data for the proton-induced nonelastic cross sections. Therefore, the second purpose is to show how to work two effects in the incident energy region and in the targets and to clarify the domain where the two effects play important roles separately in both kinds of nucleon-induced nonelastic cross sections.

II. INC MODEL**A. Ground-state and two-body cross sections**

The INC model solves a time development of a system of nucleons based on the relativistic many-body formalism with

*nakano@med.uoeh-u.ac.jp

stochastic collisions, and the cross sections are given by the assembly of probabilistic processes. The merit of the INC model is that the results are understood intuitively since all the particles can be traced in any time. In the INC model, the position and momentum of the particles in the ground state at the initial stage are prepared based on a random sampling for every injection of the nucleon. We will not repeat how to make the ground state since the method of making the ground state has been described in Ref. [16].

On the two-body cross sections, Cugnon *et al.* [18] have introduced them to reproduce the free nucleon-nucleon (NN) cross sections. Since the aim of the two-body cross sections by Cugnon is different from our aim, we introduce two-body cross sections so as to reproduce the experimental cross sections of the nucleon-induced nonelastic reactions. In the previous papers, the two-body cross sections S were given separately for the neutron injection case [16] and for proton injection case [17], however, in this paper, we propose a unified formula which can be applied to both the proton and the neutron at the same time,

$$S = Y_1 + 0.26Y_2 \quad \text{for } pp, \quad (1)$$

$$S = (Y_1 + 0.26Y_2)f_{nn} \quad \text{for } nn, \quad (2)$$

$$S = (Y_3 + 0.26Y_4)f_{pn} \quad \text{for } pn, \quad (3)$$

where the functions are given by the following and p_G is the relative momentum of the two nucleons in units of GeV/ c :

$$Y_{1a} = 29 / \{1 + \exp[-(p_G - 1.24)/0.08]\} + 19.5,$$

$$Y_{1b} = 41 + 60(p_G - 0.9)\exp(-1.2p_G),$$

$$Y_1 = Y_{1a} / \{1 + \exp[(p_G - 1.5)/0.5]\} \\ + Y_{1b} / \{1 + \exp[-(p_G - 1.5)/0.5]\},$$

$$Y_2 = 3300 \exp(-p_G^{0.8}/0.07) + 80\,000 \exp(-p_G^{0.86}/0.02),$$

$$Y_{3a} = (10p_G + 23)\{1 + 0.2 \exp[-(p_G - 0.5)/0.15]\},$$

$$Y_{3b} = 42 / \{1 + \exp[-(p_G - 1.93)/0.05]\},$$

$$Y_3 = Y_{3a} / \{1 + \exp[(p_G - 1.93)/0.05]\} + Y_{3b},$$

$$Y_4 = 8000 \exp(-p_G/0.058),$$

$$f_{pn} = 1 - 0.3 \exp[-\{(p_G - 0.5)/0.25\}^2],$$

$$f_{nn} = 1 - 0.5 \exp[-\{(p_G - 0.5)/0.25\}^2]. \quad (4)$$

Since the two-body cross sections for the nn pair are difficult to measure directly in a two-nucleon scattering experiment [19], they are not given by Cugnon. We determine our two-body cross sections so as to reproduce the experimental data in the actual INC calculations. As shown in Fig. 1, the determined two-body cross sections are the same as those by Cugnon over 1000 MeV/ c , however, smaller than those by Cugnon in the small momentum range. This reduction is considered as the medium effect in the nuclear matter [20] since it is reasonable that the interactions in the medium of the nucleus are different from the free NN interactions.

B. Coulomb repulsion

The motion of the incident proton is dominated by the total potential which is a sum of the Coulomb potential

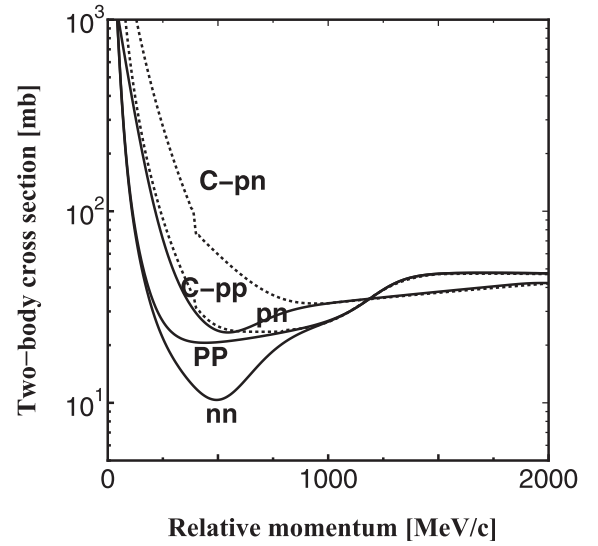


FIG. 1. Comparison of two-body cross sections between the Cugnon (dotted lines) and the proposed ones (solid lines) used in this calculation. The x axis is the relative momentum [MeV/ c], and the y axis is the two-body cross section [mb].

and the nuclear potential, on the other hand, the incident neutron is affected by only the nuclear potential. The Coulomb potential for a finite charge density is different from the point charge potential. We should calculate the Coulomb potential using the finite charge distribution. The charge distribution in the nucleus is taken as the same as the proton density of Woods-Saxon shape. The sum of the Coulomb potential and the nuclear potential of the Woods-Saxon shape is shown in Fig. 2 for ^{12}C , ^{27}Al , ^{56}Fe , and ^{208}Pb where the Woods-Saxon parameters of the Coulomb potential; the radius r_c and the diffuseness a_c are taken from the experimental data of charge distribution by electron-scattering experiments [21]; r_c [fm], a_c [fm] = 2.350, 0.540 for ^{12}C , 2.840, 0.569 for

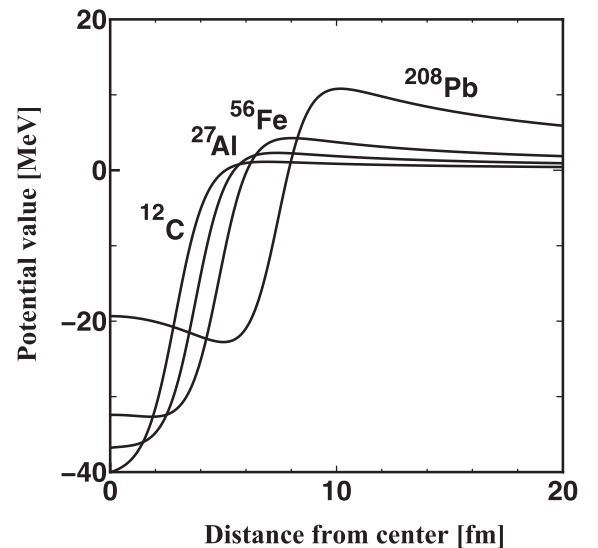


FIG. 2. The total potentials of a proton for ^{12}C , ^{27}Al , ^{56}Fe , and ^{208}Pb which sum the Coulomb potential of the finite density for a proton and the nuclear potential for a nucleon.

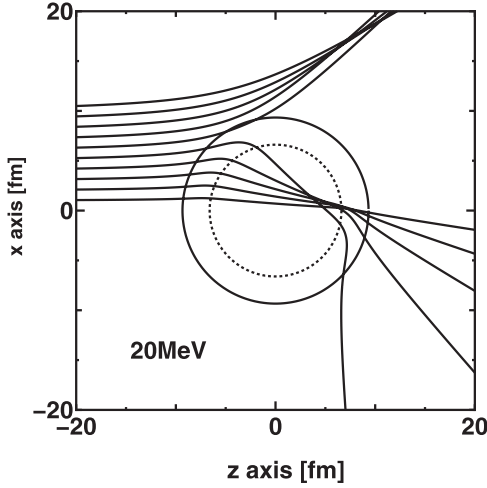


FIG. 3. Proton trajectories of the impact parameter from 1 to 10 [fm] solving the only potential scattering (without the NN collisions in the INC calculation program) under the Coulomb potential plus nuclear potential for the 20-MeV proton injected to ^{208}Pb . The dotted circle shows the radius r_n of the Woods-Saxon potential of ^{208}Pb , and the solid circle shows the radius of the maximum height of the total potential of ^{208}Pb .

^{27}Al , 4.042, 0.540 for ^{56}Fe , and 6.620, 0.546 for ^{208}Pb , on the other hand, the Woods-Saxon parameters of the nuclear potential for nucleon are taken from the global optical potential [22]; $r_n = 1.25 A^{1/3}$ [fm] and $a_n = 0.69$ [fm] with mass number A .

An example of proton trajectories of the potential scattering by the sum of the Coulomb and the nuclear potentials with no collisions is shown in Fig. 3 for the ^{208}Pb target. In order to keep the precision for solving the long-range Coulomb force, the initial point of the calculation is far from the origin; $z = -1000$ fm.

C. Discrete level constraint

In the previous papers [16,17], we pointed out that it is essential to include the constraint in the transition probability of the excited particle for the neutron- and proton-induced nonelastic cross sections. Traditionally, the naive INC model assumes that the levels are continuous over the Fermi energy. This assumption is not proper. In principle, the particle over Fermi sea should go to a discrete level with a width. We treat this effect by introducing the constraint for the excited particles. Since it is caused by the existence of discrete levels, we call it DLC, emphasizing it is not continuous. This is one example that the INC model can include quantum effects effectively. Following Ref. [16], we simulate the DLC effects in a simple way using a probability function, which represents the allowance of the excited particle going to energy E .

For the probability function, it is possible to use the shell-model orbits with widths, however, we simplified the probability by introducing the continuous function of the following shape:

$$P(E) = 1/\{1 + \exp[-(E_0 - E)/w]\}. \quad (5)$$

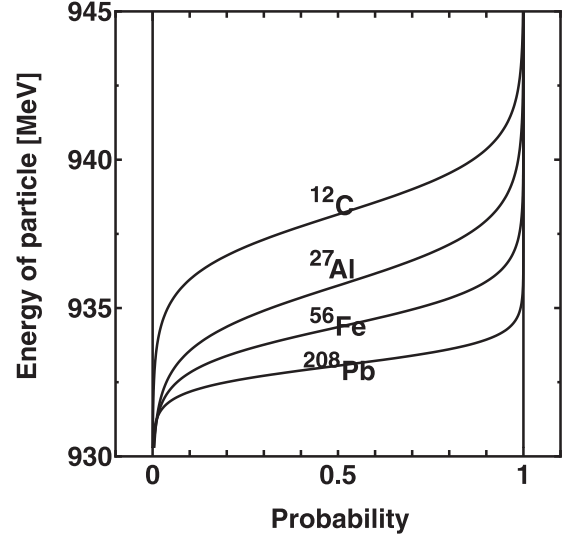


FIG. 4. The transition probability $P(E)$ used in our calculations. This figure shows the neutron case. The x axis indicates the probability from 0 to 1 for the excitation energy of the scattered particle on the y axis.

This continuous function is considered to represent a result of smoothing of the probabilities to several discrete levels with widths. The function of $P(E)$ is a so-called sigmoid curve, which is a smooth curve varying from 0 to 1. As shown in Fig. 4, the probability $P(E)$ approaches 0 as E goes to E_{Fermi} (Fermi energy) and 1 as E goes to E_{free} (free energy). The parameter E_0 in Eq. (5) is given by

$$E_0 = (E_{\text{Fermi}} + E_{\text{free}})/2 + E_{\text{th}}, \quad (6)$$

where E_{Fermi} is a nucleon-mass energy minus the binding energy; 938.92 – 8.74 MeV and E_{free} is a nucleon-mass energy; 938.92 MeV for a neutron, and 938.92 MeV + the Coulomb barrier (target dependent) for a proton.

The parameters E_{th} and w are adjusted to reproduce the curvature of the experimental data in the very low energy and listed in Table I. They are common to the proton and the neutron. They have a small target dependence showing a tendency changing gradually from the light to the heavy nuclei as shown in Fig. 4. It is noted that the essential feature of the cross sections does not largely depend on the detail of the parameters. The DLC is different from the Pauli blocking which is generally used. The Pauli blocking condition works for nucleons in the energy range of $E < E_{\text{Fermi}}$, however, the discrete level constraint does in the energy range of $E > E_{\text{Fermi}}$.

TABLE I. List of E_{th} and w for four targets.

	C	Al	Fe	Pb
E_{th} (MeV)	3.6	1.2	-0.2	-1.5
w (MeV)	1.0	1.0	0.7	0.4

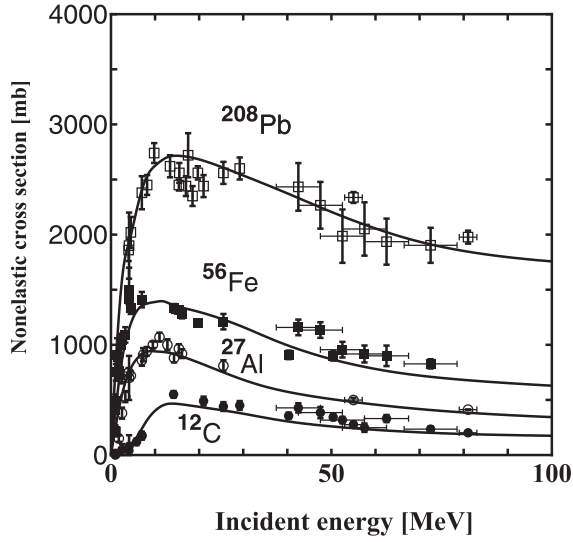


FIG. 5. Calculated results of neutron-induced nonelastic cross sections of ^{12}C , ^{27}Al , ^{56}Fe , and ^{208}Pb below 100 MeV together with the experimental data with error bars.

III. RESULTS AND DISCUSSIONS

A. Comparison of calculations including two effects

The calculated results including the two effects are shown together with the experimental data for neutron-induced nonelastic cross sections in Fig. 5 and proton-induced nonelastic cross sections in Fig. 6.

The experimental data are taken from the experimental nuclear reaction data (and references therein) [23]. The calculations reproduce the experimental data satisfactorily considering that the calculations are performed on the same basis for the wide range of targets both of neutron and of proton injection cases using the same two-body cross sections with no target dependence. Here, we note two comments to keep

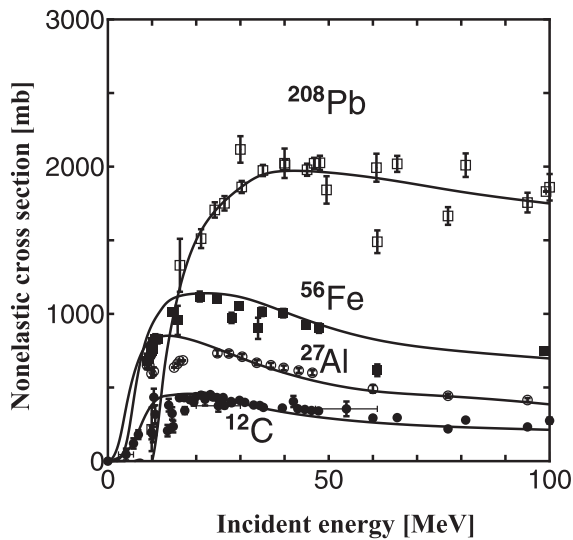


FIG. 6. Calculated results of proton-induced nonelastic cross sections of ^{12}C , ^{27}Al , ^{56}Fe , and ^{208}Pb below 100 MeV together with the experimental data with error bars.

the precision of the calculations in the extremely low-energy region below 10 MeV. The first is that the maximum range of the time development of calculations should be large since the speed of the incident particle becomes very slow. The second is that the range of impact parameters should be large since the interaction range in the low-energy region becomes very large.

Based on the reliability of the INC model, we can analyze the effects of the Coulomb repulsion and the DLC. The two types of cross sections with the two effects are expressed in the following way:

$$\sigma_n(T) = \sigma_n^{\text{bone}}(T) \varepsilon^{\text{DLC}}(T), \quad (7)$$

$$\sigma_p(T) = \sigma_p^{\text{bone}}(T) \varepsilon^{\text{DLC}}(T) \varepsilon^{\text{Coul}}(T), \quad (8)$$

where $\varepsilon^{\text{DLC}}(T)$ and $\varepsilon^{\text{Coul}}(T)$ are the reduction factors originated from the DLC and Coulomb effects at the incident energy T . When the reduction factor is set to 1, it indicates cutting the effect. We call σ^{bone} the bone structure that is determined only by the two-body cross sections cutting the effects. In the following sections, the Coulomb effects and the DLC effects for both proton and neutron injection cases are separately investigated.

B. Coulomb effect for the proton-induced reactions

In general, due to the Coulomb repulsion, the trajectories of the injected proton are bent outward as shown in Fig. 3, thus, the proton-induced cross sections are reduced significantly compared to the neutron cases. In order to show how the effect of Coulomb repulsion on the proton-induced cross sections works, we illustrate the result of the INC calculation that cuts the Coulomb repulsion. The comparison is shown in Fig. 7

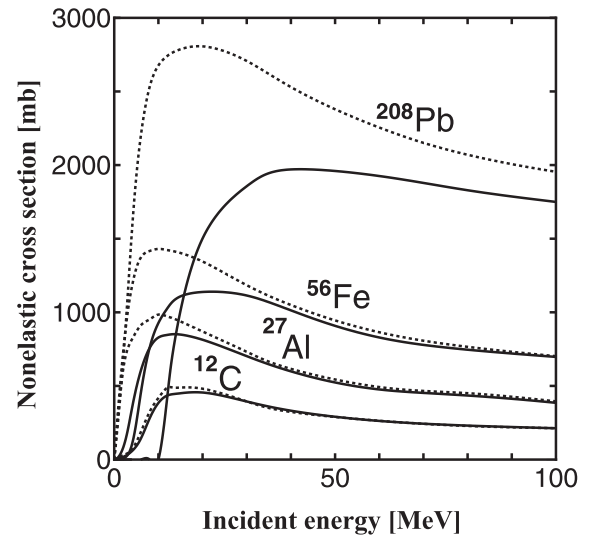


FIG. 7. Comparison between two calculations in the proton-induced nonelastic cross sections. Solid curves show the results with the Coulomb effect, and dashed curves show the results without the Coulomb effect. Since the DLC effect is included in both calculations, the difference indicates the largeness of the effect of the Coulomb repulsion.

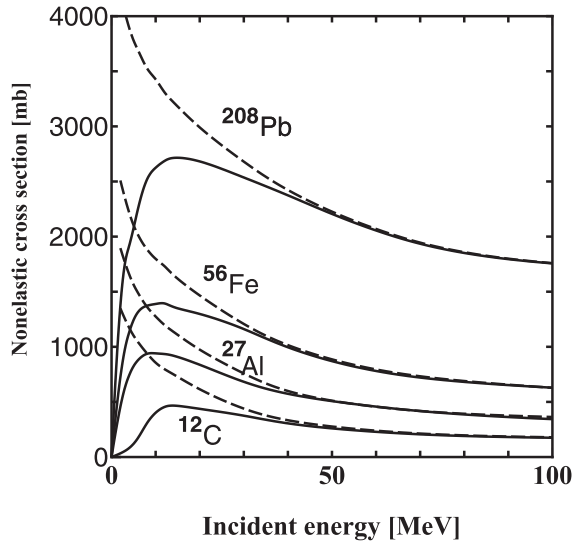


FIG. 8. Comparison between two calculations in the neutron-induced nonelastic cross sections. Solid curves show the results with the DLC effect, and dashed curves show the results without the DLC effect.

between the full calculation including the Coulomb repulsion and the calculation without the Coulomb effect. This figure indicates the Coulomb effect is extremely large for ^{208}Pb , moderate for ^{56}Fe and ^{27}Al , and very small for ^{12}C . The result can be understood from the fact that the height of Coulomb barriers including the nuclear potentials is 1.12 MeV in ^{12}C , whereas it is 10.8 MeV in ^{208}Pb which is about ten times larger than ^{12}C . On the domain where the Coulomb repulsion works, the effect is recognized to be less than around 80 MeV for ^{56}Fe and until 100 MeV for ^{208}Pb , whereas it is less than around 50 MeV for ^{27}Al and 20 MeV for ^{12}C .

C. DLC effects for neutron-induced nonelastic cross sections

Since neutron-induced nonelastic cross sections have only effects from the DLC, the cross sections without the DLC reveal the bone structure as is shown in Fig. 8, which shows the bone nonelastic cross section increases gradually as the incident energy becomes small. This structure is due to the fact that the two-body cross section increases sharply as the relative momentum decreases as is shown in Fig. 1. Figure 8 shows that the DLC effect is extremely large, which greatly changes the cross sections in the low-energy region, and the influence is observed up to around 50 MeV for ^{12}C and ^{27}Al and up to around 70 MeV for ^{56}Fe and ^{208}Pb in the neutron-induced cross sections.

D. DLC effects for proton-induced nonelastic cross sections

Next, we show the DLC effect in proton-induced cross sections by cutting off only the DLC effect. From Fig. 9, we recognize that the effect of DLC is large for ^{12}C and ^{27}Al , moderate for ^{56}Fe , and negligible for ^{208}Pb . This is just reverse to the Coulomb effects. On the domain of the effects of the DLC, the influence is observed up to around 40 MeV for ^{12}C and ^{27}Al and up to around 60 MeV for ^{56}Fe and ^{208}Pb . The

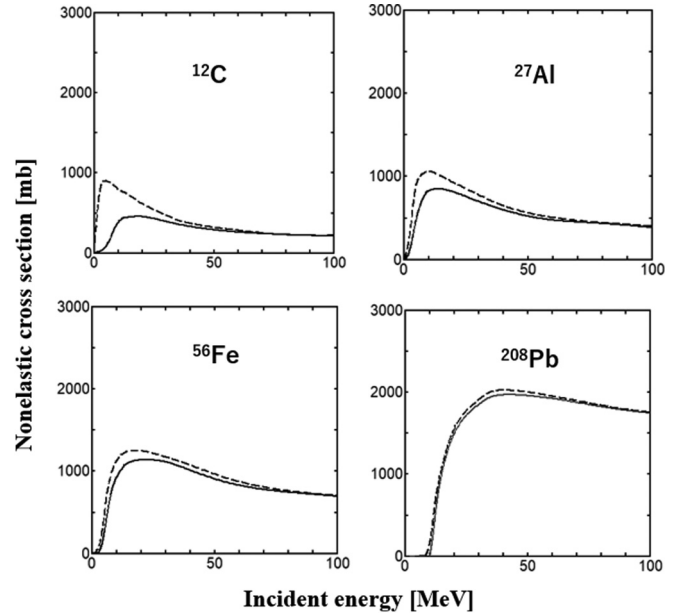


FIG. 9. Comparison between two calculations in the proton-induced nonelastic cross sections. Solid curves show the results with the DLC effect, and dashed curves show the results without the DLC effect. The difference indicates the largeness of the DLC effect.

domain of the effectiveness is similar to the neutron-induced cross sections.

IV. CONCLUSIONS

We have studied the proton- and the neutron-induced nonelastic cross sections in the low-energy region below 100 MeV. An important conclusion is that the extended INC model to include the Coulomb repulsion and the effect of the DLC can reproduce well the experimental data of the nonelastic cross sections from 100 MeV down to the very low energy of nearly 0 MeV. It is noted that the one set of the two-body cross sections which have no target dependence and no incident energy dependence can reproduce the experimental data for both neutron and proton injection cases in the wide range of the targets from ^{12}C to ^{208}Pb . The conclusion of Ref. [16] that the discrepancy between the calculations and the experiments in the low-energy region can be resolved taking into account the DLC effect is again confirmed in both proton- and neutron-induced cross sections of the wide range of targets.

As the next conclusion, on the basis of the reliability of the INC model, we analyzed the domain where the two effects play important roles. The calculations reveal the domain of the target mass and the incident energy where the two effects work largely. For the proton-induced cross sections in light nuclei, the Coulomb effect is small, instead, the DLC effect is dominant, and in heavy nuclei, the Coulomb effect is dominant, and the DLC effect is small. As for the neutron-induced nonelastic cross section, the DLC effect is especially important in the very low-energy region of all targets. We have shown that the domain where the effect of DLC works is confined below around 50 MeV for the light nuclei ^{12}C and around 70 MeV for the heavy nuclei ^{208}Pb both for the neutron and the proton.

Finally, we point out that since the domain of the DLC effect is limited to the above low energy, the traditional INC model treating nuclear reactions of higher injection energies works successfully even if it does not include the DLC effect [12,13].

ACKNOWLEDGMENT

We acknowledge Dr. G. Watanabe and the members of the Uozumi group of Kyushu University for constructive comments and encouragement during the course of this work.

-
- [1] R. Serber, *Phys. Rev.* **72**, 1114, (1947).
 - [2] J. Aichelin and H. Stocker, *Phys. Lett. B* **176**, 14 (1986).
 - [3] A. Ono, H. Horiuchi, T. Maruyama, and A. Ohnishi, *Prog. Theor. Phys.* **87**, 1185 (1992).
 - [4] J. Cugnon, *Nucl. Phys. A* **462**, 751 (1987).
 - [5] A. Boudard, J. Cugnon, S. Leray, and C. Volant, *Phys. Rev. C* **66**, 044615 (2002).
 - [6] T. E. Rodrigues, J. D. T. Arruda-Neto, A. Deppman, V. P. Likhachev, J. Mesa, C. Garcia, K. Shtejer, G. Silva, S. B. Duarte, and O. A. P. Tavares, *Phys. Rev. C* **69**, 064611 (2004).
 - [7] J. Cugnon, T. Aoust, A. Boudard, J. C. David, S. Pedoux, S. Leray, and Y. Yariv, *Adv. Space Res.* **40**, 1332 (2007).
 - [8] S. Pedoux and J. Cugnon, *Nucl. Phys. A* **866**, 16 (2011).
 - [9] S. Furihata and T. Nakamura, *J. Nucl. Sci. Technol.* **39**, 758 (2002).
 - [10] Y. Uozumi, Y. Sawada, A. Mzhavia, S. Nogamine, H. Iwamoto, T. Kin, S. Hohara, G. Wakabayashi, and M. Nakano, *Phys. Rev. C* **84**, 064617 (2011).
 - [11] Y. Uozumi, T. Yamada, S. Nogamine, and M. Nakano, *Phys. Rev. C* **86**, 034610 (2012).
 - [12] Y. Uozumi, T. Yamada, and M. Nakano, *J. Nucl. Sci. Technol.* **52**, 264 (2015).
 - [13] Y. Uozumi, Y. Yamaguchi, G. Watanabe, Y. Fukuda, R. Imamura, M. J. Kobra, and M. Nakano, *Phys. Rev. C* **97**, 034630 (2018).
 - [14] Y. Yariv, Th. Aoust, A. Boudard, J. Cugnon, J.-C. David, S. Lemaire, and S. Leray, in *Proceedings of the International Conference on Nuclear Data for Science and Technology*, edited by O. Bersillon (EDP Sciences, Paris, 2008), p. 1125.
 - [15] J. Cugnon and P. Henrotte, *Eur. Phys. J. A* **16**, 393 (2003).
 - [16] M. Nakano and Y. Uozumi, *Phys. Rev. C* **100**, 034619 (2019).
 - [17] M. Nakano, Y. Yamaguchi, and Y. Uozumi, *Phys. Rev. C* **101**, 044616 (2020).
 - [18] J. Cugnon, D. L. Hote, and J. Vandermeulen, *Nucl. Instrum. Meth. Phys. Res. Sect. B* **111**, 215, (1996).
 - [19] W. N. Hess, *Rev. Mod. Phys.* **30**, 368 (1958).
 - [20] N. J. DiGiacomo, R. M. DeVries, and J. C. Peng, *Phys. Rev. Lett.* **45**, 527 (1980).
 - [21] H. De Vries, C. W. De Jager, and C. De Vries, *At. Data Nucl. Data Tables* **36**, 495 (1987).
 - [22] R. L. Varner, W. J. Thompson, T. L. McAbee, E. J. Ludwig, and T. B. Clegg, *Phys. Rep.* **201**, 57 (1991).
 - [23] Experimental Nuclear Reaction Data (EXFOR), <https://www.jcprg.org/exfor/>.